Anion···π interactions and metastability: structural transformations in a silver-pyrazine network

William J. Gee,*[a,b] Karen Robertson[a] and Jonathan M. Skelton[a]

Dedication ((optional))

Abstract: Structural evidence of anion···π interactions influencing single-crystal-to-single-crystal (SCSC) transformations is demonstrated herein with a metastable silver-pyrazine system. A cascade of SCSC transformations driven by changes to anion···π stabilisation sees two metastable species convert to a ground-state form. This constitutes one of the most dramatic chemical effects yet attributed to anion···π interactions. The metastable networks, [Ag(μ-NO_2)(pyz)] (**1**-**2**), are composed of dimerised (**1**) and delaminated (**2**) $AgNO_2$/pyrazine, which convert to the ground-state [Ag(κ^2-NO_2)(pyz)] form (**3**) with 3D connectivity. The metastable phases show responsiveness to solvent vapour and temperature. This work shows how anion···π interactions influence solid-state structure with support from computational modelling, and highlights how metastable materials may harness anion···π interactions to deliver large structural and property changes.

Introduction

Interest surrounding anion···π interactions has rapidly evolved from questioning the fundamental existence of such interactions,[1] to detailed investigations of solution[2] and solid-state[3] behaviour supplemented by high level *ab initio* computational modelling.[4] While controversy surrounding proper nomenclature of these interactions is ongoing,[5] the importance of anion···π interactions to a wide range of chemical processes is undisputed. Recent illustrative reports include the stabilisation of biomolecules,[6] promotion of catalysis,[7] and the creation of new ion-transport systems.[8] Consequently these weak interactions extend the design-toolbox available to the crystal engineer,[9] despite their specialised nature.[10]

Aromatic systems tailored for anion···π interactions in the solid-state can be engineered by attaching strong electron-withdrawing groups to the ring, or by incorporating electronegative heteroatoms. Pyrazine (pyz)-silver coordination-polymer systems have proved a reliable means of harnessing such interactions, as evidenced by several past reports.[4,11] These related structures containing anion···π interactions serve as the inspiration for the design of new materials.

In addition to being amenable to anion···π interactions, Ag-pyz frameworks possess silver nodes capable of forming argentophilic interactions, providing a second means to direct the structure in the solid state. This capability stems from the high degree of coordinative flexibility available to monovalent silver complexes, coupled with weaker relativistic effects.[12] Examples harnessing Ag···Ag interactions include the fusing of interpenetrated 2D sheets within a coordination polymer,[13] the promotion of self-assembled helicate materials,[14] and the ordering of chains of aromatic bridging ligands in the solid state.[15]

By targeting materials that support varying combinations of weak interactions with similar energies (e.g. π···π, δ^-···π, and Ag···Ag), the likelihood of isolating systems with metastable phases is increased. Furthermore, by engineering weakly-interacting linear coordination-polymer chains barriers to solid-state reorganisation such as interpenetration can be suppressed. These ideas were borne out in our previous work with rod-like linear silver complexes.[16]

Techniques for synthesising metastable materials are both topical and highly sought after, with refinements to processing techniques having resulted in new and innovative ways of imparting metastability.[17] The drive to create new metastable materials stems from an ever-growing range of applications including pharmaceutical formulations with improved bioavailability,[18] sensors derived from photoswitchable compounds,[19] and switchable molecular magnets.[20] Our recent efforts have explored bottom-up approaches to obtain inherently metastable materials that harness the interchangeability of first and second coordination-sphere bonding to metal nodes.[21]

Here the metastable properties of silver-pyrazine coordination polymers are explored using two newly identified metastable phases that are stabilised by anion···π interactions, each of which undergoes SCSC conversion to a more stable conformer. Both SCSC transformations involve large changes to the molecular arrangement, and we demonstrate that the speed of the changes can be influenced by the presence of certain solvent vapours and by temperature, providing a measure of control to this process. To the best of our knowledge, this work represents the first example of metastable materials harnessing anion···π interactions for functionality, providing valuable insights to both areas of research.

[a] Dr W. J. Gee, Dr K. Robertson, Dr J. M. Skelton
Department of Chemistry, University of Bath,
Claverton Down, Bath BA2 7AY, (UK).
[b] School of Physical Sciences, University of Kent, Canterbury,
Kent, CT2 7NH, (UK).
Email: W.Gee@kent.ac.uk

Supporting information for this article is given via a link at the end of the document. Synthesis and characterisation details; conversion behaviour (**1** → **3**) in acetonitrile; photos of **1**-**3**; an expanded discussion and depiction of Figure 3; details of the variable-temperature PXRD experiment showing direct **1** → **3** conversion; DSC data obtained for **1**; detailed assignment of the estimated conversion% upon exposure to specific solvent vapours; the UV-Vis DRS spectra for **1**-**3**; and the first-principles modelling of the optical properties of **1**-**3**.

Results and Discussion

Design

A key requirement for anion···π interactions is a positive quadrupole moment within the aromatic system.[2] Coordinating silver nodes to pyridyl ligands is one strategy that has been employed with considerable success.[4,11g-h] Computational modelling shows that both isolated pyz molecules and molecules coordinated to Ag nodes possess two types of electron-deficient region that could facilitate weak electrostatic interactions with anions, *viz.* at the ring protons, and in the π-electron cloud above the C atoms (Fig. 1).

While counter-anion identity will influence the crystalline product, linear chains of alternating silver/pyrazine are a ubiquitous motif,[11a-f] making the resulting solid-state structures somewhat predictable. Nitrite (NO_2^-) was chosen as the counter-ion for this study to provide a hard base with established metastable functionality.[22] The formation of an $AgNO_2$/pyz coordination polymer has been demonstrated using hydrothermal synthesis.[15c] However, this approach would disfavour the formation of metastable species comprised of weak interactions such as anion···π interactions, and consequently we eschew harsh hydro- and solvothermal synthesis in this work and instead employ mild crystallisation conditions. A complete synthetic procedure may be found in the Electronic Supplementary Information (ESI, Section S1).

Stability of the metastable species

Combining acetonitrile solutions of $AgNO_2$ and pyz at ambient temperature results in rapid precipitation of yellow needle-like crystals of the metastable coordination network, [Ag(*μ*-NO_2)(pyz)] (**1**). Once formed, crystals of **1** suspended in solution convert within 30 mins to the known thermodynamically-stable network structure [Ag(*κ*^{2}-NO_2)(pyz)] (**3**) (ESI, Sections S2).[15c] Rapid isolation of **1** from the mother liquor with drying stabilises the crystals for analysis. Over the course of days, the isolated yellow metastable crystals lose colour, with subsequent investigation (*vide infra*) revealing conversion to a second metastable coordination species (**2**). **2** possesses identical composition to **1**, *i.e.* [Ag(*μ*-NO_2)(pyz)], but shows marked differences in second coordination-sphere bonding of the metal, and in the orientation of the pyz ligands. After *ca* two weeks metastable form **2** undergoes near-quantitative conversion to the ground-state form **3**. Images of as-synthesised **1**, intermediate **2**, and ground-state **3** are available in the ESI (Section S3).

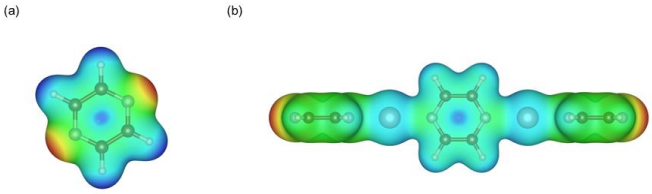

Figure 1. Electrostatic potential maps of the pyrazine molecule (a) and the trimeric Ag aggregate (b). Red regions indicate areas of high negative charge, while blue regions indicate positively-charged areas. Pyrazine has two potential sites for interaction with anions, *viz. via* C-H···anion interactions, and *via* electron-deficient patches on the π-electron system above the C atoms. Both features are preserved on coordination to Ag.

Crystallographic and computational analysis

Figure 2 shows the crystal structures of **1**-**3** alongside calculated electrostatic potential maps highlighting the anion···π and anion···H interactions.

1 adopts the orthorhombic space group *Pnma* and consists of a 2D sheet motif of zig-zagging chains of Ag^+/NO_2^-, wherein each nitrite bridges between two silver nodes in a *μ*-[*κ*^{2}-O:NO] manner (Fig. 2a/2b). The chains are linked by pyz ligands, each of which bridges two Ag centres. The Ag atoms exhibit four first coordination-sphere interactions (here defined as an Ag-X bond length of less than 2.54 Å),[23] namely the symmetry-equivalent pair Ag(1)-N(1) and Ag(1)-N(1') (*d* = 2.329(4) Å), Ag(1)-O(1) (*d* = 2.499(4) Å), and Ag(1)-O(1") (*d* = 2.437(5) Å). Two weaker, second coordination-sphere interactions between the NO_2^- ligands and adjacent Ag atoms were also evident between Ag(1)-O(2) (*d* = 2.7546(12) Å) and Ag(1)-N(2"') (*d* = 2.7011(14) Å). Symmetry operators ('): *x*, ½ - *y*, *z*, ("): ½ + *x*, ½ - *y*, ½ - *z*, ("'): *x* - ½, ½ - *y*, ½ - *z*.

The relative orientation of the pyz ligands within each 2D sheet resembles the herringbone pattern, with every second pyz molecule rotated by 58° when viewed down the crystallographic *a* axis. This allows the electron-deficient aromatic hydrogens on the pyz ring to interact with electron-rich O atoms of nitrite anions in the adjacent sheets. Anion···π interactions occur between the sheets, from the non-coordinated oxygen atoms of the nitrites to the electron-deficient aromatic pyz rings in neighbouring sheets (O(2)···pyz ring/plane distance = 3.123 Å; Fig. 2b).

This analysis is supported by electrostatic-potential maps obtained from computational modelling (Fig. 2c), which clearly show anion···H-C and anion···π interactions between adjacent sheets (d_O···H-C = 2.538 Å, d_O···C(pyz) = 3.129 Å in the optimised model). Strikingly, the electron-deficient regions of the π system above the C atoms appear to be enhanced in the solids compared to in the isolated molecule and Ag-pyz aggregate (*c.f.* Fig. 1), suggesting that the anion···π interactions are enhanced in the solid, presumably due to changes in the electron distribution around the pyz ligands in the extended network.

Air drying **1** for between two and five days afforded substantial conversion to **2**. X-ray diffraction analysis revealed a decrease in symmetry to the monoclinic space group $P2_1/m$. The structure of **2** is a delaminated 2D net that results from rearrangement of the silver-nitrite bonds in **1** (Fig. 2d/2e). Each silver node in **2** is ligated by two pyz and two NO_2^- ligands. The anion bridges the silver nodes in a *μ*-[*κ*^{1}-O:*κ*^{1}-N:O] fashion, with the non-coordinating oxygen atom just beyond the covalent-bonding distance at 2.613(4) Å. The remaining covalent interactions linking the silver node are Ag(1)-N(1) and Ag(1)-

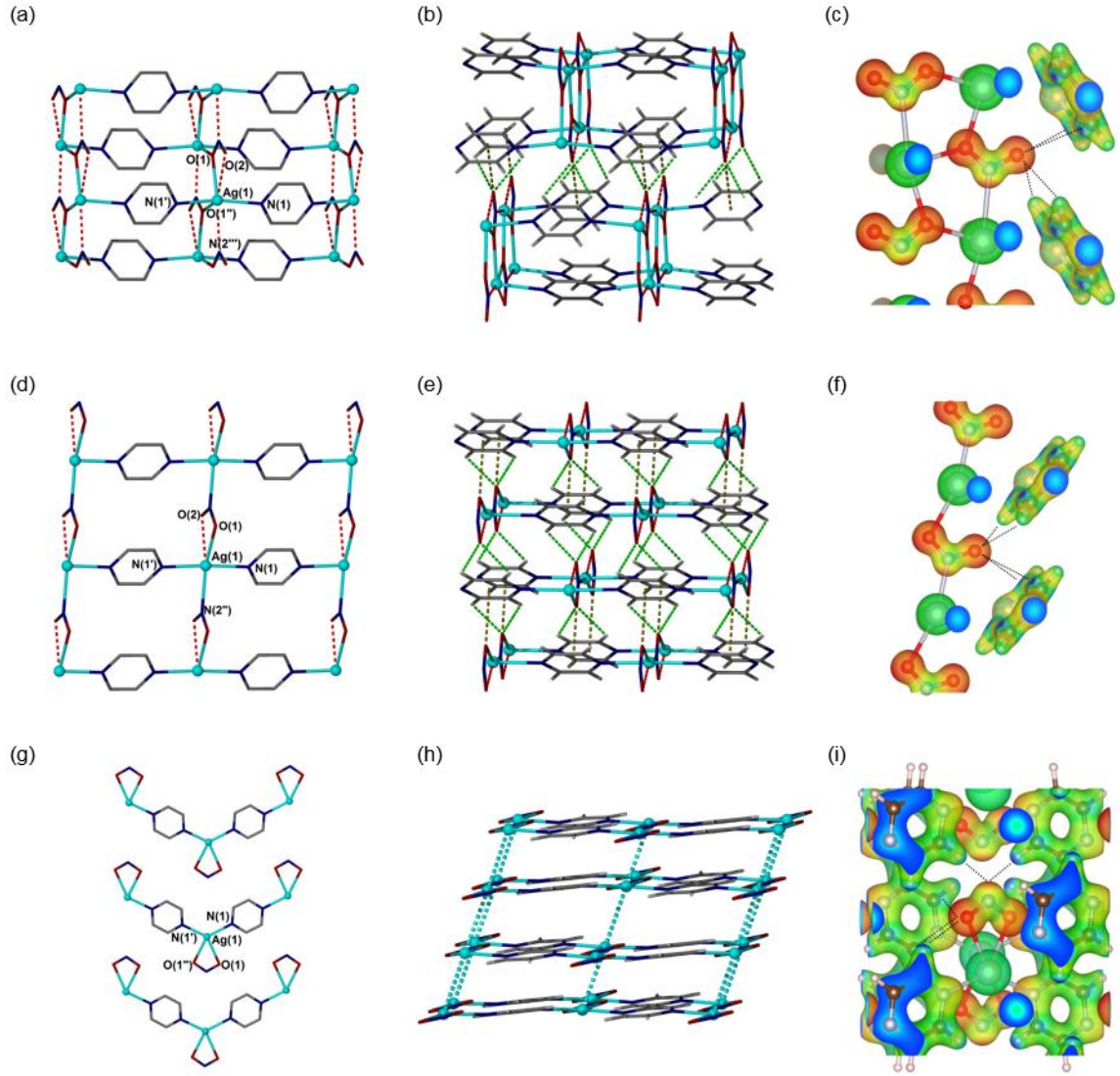

Figure 2. X-ray structures and weak interactions in metastable **1** (a-c) and **2** (d-f), and ground-state **3** (g-i). The 2D sheet motif of **1** results from the coordination of two pyrazine ligands and three nitrite anions to each silver node by covalent and non-covalent bonds (a). Individual sheets of **1** are linked by anion···π interactions between pyrazine and nitrite (gold dashed lines) and anion···H-C interactions (green dashed lines) (b). Delamination of the 2D sheet motif yields **2**, resulting in silver nodes coordinated by two pyrazines and two nitrite anions (d). Delamination does not occur in the region of the anion···π and anion···H-C interactions; instead, covalent silver-nitrite bonds are exchanged for additional anion···H-C interactions (e). The chain motif of **3** consists of silver nodes ligated by two pyrazine ligands and a single capping nitrite anion (g). The 1D chains are crosslinked by Ag···Ag interactions (h). The structural data for **3** was obtained from a previous report (CCDC: 440/081).[15c] Calculated electrostatic-potential maps for each structure (c-i) confirm the presence of anion···π and anion···H-C interactions.

N(1') (d = 2.345(3) Å), Ag(1)-O(1) (d = 2.531(4) Å), and Ag(1)-N(2") (d = 2.507(4) Å) (symmetry operators ('): x, ½ - y, z, ("): x - 1, y, z).

Unlike the precursor material, the orientations of all the pyz ligands in **2** are aligned. Two distinct weak interactions involving the pyrazine molecules are present (Fig. 2e), *viz.* anion···π interactions on one terminus of NO_2^-, analogous to those in **1**, and an electrostatic interaction between the aromatic ring protons of pyz with the other terminus. These inter-sheet stabilising interactions alternate in the direction of the crystallographic c axis (Fig. 2e). Computational modelling (Fig. 2f) confirms the presence of the weak interactions (d_O···H-C = 2.508 Å, d_O···C(pyz) = 3.260 Å), and again shows an enhanced electron depletion above the C atoms in the pyz π system. Compared to **1**, there is a shortening in the anion···H-C distance and a lengthening of the anion···π distance, which, together with the other structural changes, presumably contributes to the higher stability of **2**.

Conversion of the air-dried material to the thermodynamically-stable **3** was deemed complete based on powder-diffraction evidence after 15 days. Characterisation performed on this material matches that of the previous report.[15c] The 2D network is lost due to the nitrite adopting a capping mode as opposed to bridging (Fig. 2g). The formerly linear pyz-Ag-pyz bond angle of **2** (N(1)-Ag(1)-N(1') = 175.28(13)°) becomes bent in **3** (N(1)-Ag(1)-N(1') = 125.98°) to allow for Ag···Ag interactions to link the chains into a 3D framework (Fig. 2h).

Analysis of the calculated electrostatic potential (Fig. 2i) reveals multiple potential weak interactions. The O atoms on the NO_2^- anion could potentially participate in C-H···anion interactions with the H atoms on pyz rings within the chains (d_O···H-C = 2.445 Å), and also in anion···π interactions with pyz ligands in the sheets below and above (d_O···C(pyz) = 3.504/3.561 Å). The N atom can also participate in C-H···anion interactions with adjacent chains within the same sheet (d_N···H-C = 2.373 Å). As for the **1** → **2** transition, there is a reduction in the length of the C-H···anion interaction distances and a lengthening of the anion···π interactions. We also find that the most electron-deficient region of the pyz rings in form **3** is at the ring protons, as in the molecule (*c.f.* Fig. 1a), rather than above the C atoms as in **1** and **2**, suggesting that changes to the bonding network in **3** further reduces the propensity for the weak anion interactions.

Characterising transformations to the ground state

Yellow needles of **1** were found slowly to convert to **2** *via* a SCSC transformation when isolated and dried following crystallisation. The nature of this conversion was probed over 15 days using powder X-ray diffraction (PXRD) analysis (Fig. 3). Both the t = 0 and t = 15 day patterns matched references simulated from the single-crystal structures of **1** and **3**, demonstrating homogenous start and end points. Minor variations in peak height and position relative to the references were noted, but could be attributed to differences in the collection temperature (298 and 150 K for the PXRD and single-crystal collections, respectively) as well as to a high probability of non-random crystal orientation in the powder. The latter is due to observed mechanochemical conversion of **1**/**2** to **3**, which precluded sample grinding. These caveats aside, complete conversion of **1** was observed after 3 days coincident with the appearance of a transient peak at a 2θ angle of *ca* 16°, confirmed to be an indicator of the conversion to **2** based on a reference pattern derived from the crystal structure (see ESI, S4). After 10 days the majority of **2** had converted to **3**, with only trace amounts present at day 15, at which point the SCSC conversion was deemed complete.

Direct SCSC conversion of **1** → **3** could also be triggered by heating. A variable-temperature PXRD experiment showed that heating a capillary loaded with **1** from a base temperature of 323 K (50 °C) in 10 K increments to 400 K (127 °C) results in complete conversion to **3** by 393 K (120 °C). The onset of conversion occurs within the range of 353-363 K (80-90 °C).

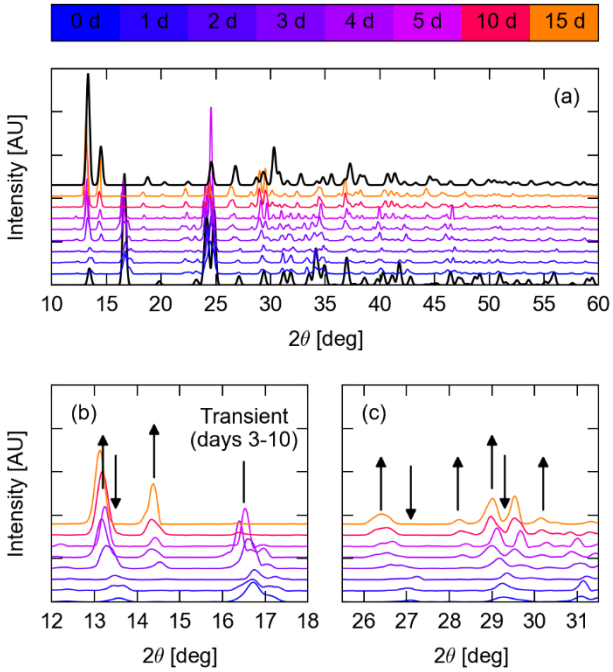

Figure 3. Powder X-ray diffraction (PXRD) analysis of the single-crystal to single-crystal transformations. (a) PXRD patterns recorded between 2θ angles of 10 and 60°. The series starts with a reference pattern of **1** (black, bottom), continues with experimental patterns collected from 0 to 15 days (blue to orange), and finishes with a reference pattern of **3** from a single-crystal structure solved in the monoclinic space group *Cc* (black, top). (b, c): Expansions of the experimental PXRD patterns between 12-18 and 25.5-31.5°, highlighting the appearance and disappearance of peaks during the conversion of **1** → **2** → **3**. A transient peak observed between 3 and 10 days (b) evidences the intermediate phase between **1** and **3**. This figure is expanded in the ESI, Section S4.

Further details are provided in the ESI (section S5). This was supported by DSC measurements performed on a fresh sample of **1** (see ESI, S6), which showed an irreversible phase change occurring with an onset temperature of 80 °C and reaching completion at 120 °C after eight minutes. Finally, the SCSC conversion of **1** to **3** could also be visualised using microscopy; a video demonstrating the 'molecular domino' effect[24] during the temperature-induced SCSC transformation is available as extended data.

Effect of chemical vapour on the SCSC transformations

Freshly-prepared dry crystalline samples of **1** were sealed in environments containing partitioned reservoirs of a selected solvent (Table 1) and compared with a control batch stored in air. PXRD was performed after 2 and 24 hours to estimate the conversion by comparing the relative areas of diagnostic peaks. It should be emphasised that preferred crystal orientation will have an influence the peak intensities in the PXRD data, and hence we only comment on general trends. The method for conversion ratio estimation is provided in the ESI, Section S7.

Table 1. Effect of solvent vapour on the % conversion of **1**

				Estimated conversion after 2 hours[a]		Estimated conversion after 24 hours[a]	
Entry	Solvent	Coordinating ability (a^{TM})[b]	Dielectric constant (ε)	Form **2**	Form **3**	Form **2**	Form **3**
1	none[c]	-	-	<5	0	44	0
2	water	-0.1	78.54	11	89	0	100
3	DMF	-0.2	38.25	7	93	0	100
4	acetonitrile	-0.2	36.64	5	95	0	100
5	THF	-0.3	7.52	64	0	20	32
6	methanol	-0.4	32.6	29	0	47	23
7	ethanol	-0.5	24.6	21	0	89	0
8	toluene	-1.2	2.38	33	0	73	0
9	diethylether	-1.4	4.26	22	0	71	0
10	hexane	-1.8	1.89	<5	0	38	0

[a] Estimated conversion ratios of form **1** to forms **2**/**3** derived by comparing peak areas under diagnostic peaks from the powder X-ray diffraction (PXRD) analyses: 2θ = 16.7° (**1**, [101]), 16.4° (**2**, [100]) and 13.2° (**3**, [110]). Full details of the conversion ratio calculations are provided as ESI, Section S7. [b] Coordinating ability to transition metals (a^{TM}); larger negative values denote a lower tendency to coordinate.[25] [c] Crystals of **1** stored in air.

A large increase in the SCSC transformation rate was observed when crystals of **1** were exposed to acetonitrile, water or *N*,*N*-dimethylformamide (DMF) vapour. Estimated conversion of **1** to **3** ranged from 89–95% after only two hours in the presence of these solvents (Table 1, entries 2–4), compared with no appreciable conversion for the control sample in air. After 24 hours complete conversion to ground state form **3** was observed with these solvents. A range of other common solvents were also investigated (Table 1, entries 5–10) and, with the exception of hexane (Table 1, entry 10), each was found to impart a slight increase in the rate of conversion to both **2** and **3** relative to the control.

These results show that polar, coordinating solvents (Table 1, entries 2–4) accelerate the conversion of the metastable species to the ground state. It appears that both the coordinating ability and dielectric constant of the solvent influence the transformation. The solvents shown in Table 1 have been ranked according to their ability to coordinate transition metals (a^{TM}),[25] a score where more negative values denote a poorer tendency to form coordination complexes. The three solvents with the highest score produce the largest increase in the rate of SCSC transformation (Table 1, entries 2–4). These three solvents also possess the largest dielectric constants, and as such would screen the weak electrostatic interactions that stabilise each structure upon coordination. Poor coordination ability explains why methanol (Table 1, entry 6), which possesses a similar dielectric constant to acetonitrile and DMF, shows similar reactivity to less polar solvents.

These results unambiguously demonstrate that **1** is responsive to acetonitrile, water and DMF vapour, by rapid conversion to ground-state **3**. This can be observed visually by a change in crystal colour from yellow to colourless. A plausible explanation is that the new electrostatic interactions formed by coordination of these solvents to the exposed metal nodes at the crystal faces lowers the energy barrier preventing dissociation of the silver-nitrite bonds, thus making the molecular rearrangements necessary for the transformation significantly more facile.

Mechanism of the SCSC transformations

The crystallographic data enables us to postulate a plausible mechanism for the cascade of SCSC transformations initiating from metastable **1** and concluding at the known ground-state **3**.[15c]

Focussing on the initial transition of **1** → **2**, an identical array of weak anion···{π, H-C} interactions are present in both structures (Fig. 4a, green) providing a frame of reference for the structural changes. To achieve the delamination of **1**, the silver-nitrite covalent bonds must be broken (*d* = 2.499(4) Å; Fig. 4a, red). The energetic driver for this reaction is likely the release of strain identifiable as bowed coordination of pyrazine. The conversion to **2** linearizes the angle made between the silver atoms and the centroid of the pyz ring, which is 170 and 177° in **1** and **2**, respectively.

Delamination allows the alternate sheets in **2** to undergo translation (Fig. 4a, blue) in conjunction with reorientation of pyz (Fig. 4a, pink) and nitrite ligands to form new anion···H-C interactions. The pyrazine ligands rotate by 49°, most likely assisted by electrostatic interactions with the nitrite anion. Half of the green highlighted regions swivel upon delamination to achieve greater ordering. This occurs as a cascade of molecular reorganisation throughout the crystal with the retention of single-crystallinity.

The second SCSC transformation from **2** to **3** results in further weakening of the anion···{π, H-C} interactions in favour of argentophilic Ag···Ag interactions. This likely occurs by a second translation event in which every second sheet of **2** (Fig. 4b, blue) shifts to bring the silver nodes into alignment. Whereas in **2** the pyz-Ag-pyz coordination is close to linear ($\angle_{N\text{-}Ag\text{-}N}$ = 175.28(13)°), the coordination in **3** is bent with an equivalent angle of 126°.[15c] This narrows the $\angle_{N\text{-}Ag\text{-}N}$ coordination angle, providing space in the lattice for the nitrite anion to twist and chelate the silver node, forming a sawhorse junction. The 1D chain motif formed by pyz and nitrite is almost planar, which improves the stacking efficiency of the individual chains in the crystal and maximises the Ag···Ag interaction (Fig. 4c).

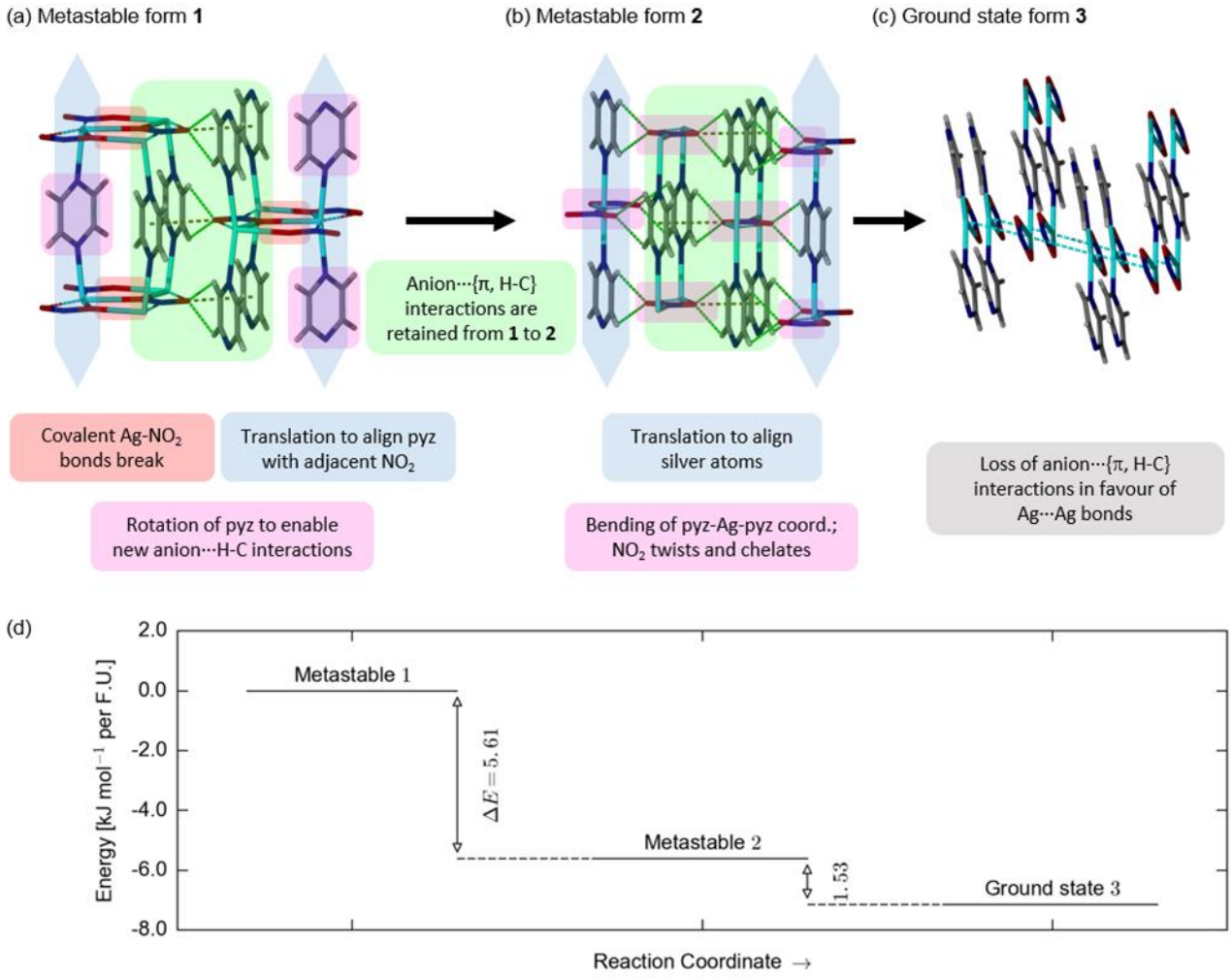

Figure 4. Proposed mechanism for the sequential **1** → **2** → **3** single-crystal to single-crystal (SCSC) transformation. (a) Comparison of the crystal structures of **1**, **2** and **3** reveals commonalities that enable an SCSC transformation mechanism to be postulated. A consistent motif of anion···{π, H-C} interactions in **1** and **2** (highlighted in green) provides a frame of reference. The transformation from **1** → **2** → **3** can be explained as a series of 2D network translations (shown in blue) and bending of the coordination about the silver atoms (pink). (b) Energetics calculations performed with dispersion-corrected density-functional theory yield energy differences of 5.61 and 1.53 kJ mol^{-1} per F.U. for the **1** → **2** and **2** → **3** transformations, respectively.

Comparison of the total energies of **1**, **2** and **3** obtained from the calculations (Fig. 4d) yield energy differences of 5.61 and 1.53 kJ mol^{-1} per F.U. for the conversions **1** → **2** and **2** → **3**, respectively, suggesting the initial metastable product **1** to lie 7.14 kJ mol^{-1} per F.U. above the final form **3** in energy. These energy differences are of the order typical for crystalline polymorphs displaying differences in other weak interactions such as H-bonding, halogen bonding and π-stacking.[26] We note however that these calculations do not provide access to the kinetic (activation) barriers for the transformations.

The mechanism proposed above supposes that the SCSC transformation cascade from **1** to **3** proceeds *via* intermediate **2** which, based on PXRD analysis (*c.f.* Fig. 3), is true at ambient temperature. This cascade of SCSC transformations conforms to Ostwald's rule,[27] in that inherently metastable phases transform to states with the closest energy, as opposed to states that are the most thermodynamically stable. Imparting anion···π interactions into the solid-state structure likely improves the likelihood of obtaining a metastable phases by multiplying the number of possible combinations of weak stabilising forces suitable for crystalline lattice formation of the material. Provided mild synthesis conditions are employed, isolation of structures with low activation energy barriers to conversion becomes more probable. This, in turn, results in a greater synthetic chance of observing facile solid-state conversion to a more stable conformer for this type of material.

Optical Properties of 1-3

The transformation of **1** → **3** occurs with a visible change in crystal colour from yellow to colourless. To quantify this, UV-visible diffuse-reflectance spectroscopy (DRS) profiles were

collected for samples of **1**-**3**. The analysis showed that the yellow colour is retained upon conversion of **1** → **2**, and that the conversion to the ground-state **3** is responsible for the loss of colour. The UV-vis DRS spectra are provided as ESI, Section S8.

Crystalline sample **1** does not absorb light at wavelengths longer than 550 nm, but the absorption increases sharply between 400-500 nm, reaching a maximum at 380 nm that then plateaus to 250 nm. Crystals of **2** made by aging a sample of **1** in air for three days showed similar absorption properties. **3** absorbs similarly in the UV, but the absorption rapidly declines between 380-420 nm, then tapers gradually to zero at 750 nm.

Absorption spectra obtained from hybrid electronic-structure calculations on the optimised models reproduce qualitatively the similar absorption profiles of **1** and **2** and the blue-shifted absorption of **3** (see ESI, S9). The onset of the absorption correlates well with the size of the bandgap between the highest-energy occupied and lowest-energy unoccupied crystal orbitals (HOCO/LUCOs), suggesting that an analysis of the frontier orbitals would shed light on the microscopic origin of the colour change. **1** and **2** have similar HOCOs and LUCOs, corresponding to orbitals delocalised over the Ag-NO_2 chains and on the pyz π system, respectively (see ESI, S9). This leads to similar direct bandgaps of 2.930 and 2.646 eV, respectively. On the other hand, whereas the LUCO in **3** is similar to those in the metastable species, the HOCO is significantly altered due to the changes in the NO_2 coordination and the Ag···Ag bonding, resulting in a considerably larger bandgap of 3.638 eV.

The changes in optical absorption between **1/2** and **3** highlight an additional dimension in engineering weak interactions, *viz.* the possibility of fine-tuning optical properties by perturbing frontier orbitals.

Conclusions

Detailed study of the new metastable forms of the [Ag(NO_2)(pyz)] coordination polymer has revealed that the facile cascade of SCSC transformations to a known ground-state form[15c] occurs at the expense of anion···π interactions. The contribution of the anion···π interactions to the stability in each structure decreases from **1** → **2** → **3**, clearly evidenced by a lengthening of the anion···π distances in favour of stronger anion···H-C and Ag···Ag interactions. This suggests that materials designed to include anion···π interactions will have a high propensity for metastability and SCSC transformations as observed here. This work thus represents the first application of anion···π interactions in the design and engineering of metastable coordination polymers.

The structural and computational analysis of **1** and **2** has allowed a plausible mechanism for the sequence of SCSC transformations ending with the ground-state **3** to be proposed. The SCSC process provides new insights into the strength of anion···π interactions relative to other, more widely-used tools in crystal-engineering.

The metastable materials reported in this study were found to be responsive to multiple stimuli, *viz.* temperature and certain types of solvent vapour, which resulted in a colour change through conversion to the ground state. This provides scope for the development of sensors and other 'smart' switchable materials based on kinetically-trapped metastable states such as those described here. In broader terms, the demonstration of anion···π interactions playing an active role in facilitating the response of a functional material to environmental stimuli complements similar breakthroughs in anion transport and molecular recognition, and will pave the way for future developments in this new area of research.

Experimental Section

General. Chemicals and solvents used for synthesis were obtained from Sigma-Aldrich and used without further purification. FT-IR spectra were recorded at room temperature in the range 4000–600 cm^{-1} using a PerkinElmer FTIR spectrometer with an ATR sampling accessory. DRS measurements were performed from 250-800 nm using a Shimadzu UV-2600 spectrometer in reflectance mode. DSC studies were performed using a Thermal Advantage Q20 DSC equipped with Thermal Advantage Cooling System 90 and operated with a dry nitrogen purge gas at a flow rate of 18 cm^3 min^{-1}. 2–4 mg samples were placed in sealed Tzero aluminium pans and heated at a rate of 2.5 K min^{-1}. Analysis of the data was carried out using the TA Universal Analysis software.

Synthesis of 1. Combining two acetonitrile solutions (1.0 mL) of pyrazine (50 mg, 0.62 mmol) and silver nitrite (123 mg, 0.80 mmol) results in instantaneous precipitation of microcrystalline **1** [Ag(*μ*-NO_2)(pyz)]. The microcrystals were isolated by filtration and rapidly washed with diethylether (3 x 5 mL) before drying under a flow of dry nitrogen gas to yield yellow crystals of **1**. Single crystals suitable for X-ray diffraction studies were obtained by diluting the precursor solutions to 2.0 mL, retarding precipitation and increasing the crystallite size. Yield: 130 mg (89 %); m.p. 80 °C (phase transition); IR (ATR): ν_{max} = 3088 (w), 1480 (w), 1414 (m), 1229 (s), 1152 (s), 1119 (s), 1068 (m), 1039 (s), 847 (w), 810 (s) cm^{-1}. Bulk purity was confirmed by PXRD measurements (see ESI).

Synthesis of 2. High purity (> 95%) **2** was obtained by sealing a sample of **1** in an enclosed vessel containing a portioned reservoir of ethanol for 30 hours. Alternately, ageing a sample of **1** in air for two days also yielded an enriched sample of **2**, but with small amounts of **3** detectable by PXRD. Single crystals of **2** suitable for X-ray diffraction studies were obtained using the air-drying method. IR (ATR): ν_{max} = 3105 (w), 3040 (w), 1488 (w), 1417 (m), 1227 (s), 1152 (s), 1120 (s), 1085 (w), 1045 (s), 993 (w), 847 (w), 810 (s) cm^{-1}. Bulk purity was confirmed by PXRD measurements (see ESI).

Crystallography. Single-crystal diffraction data for **1** and **2** were collected on an Agilent SuperNova EosS2 diffractometer using a standard Cu microfocus source (λ = 1.54184 Å). The crystals were kept at 150(2) K during collection using an Oxford Cryosystems Cryostream Plus. Using XSEED,[28] the structures were solved with SHELXS[29] and refined by full-matrix least-squares on F^2 using SHELXL-2014.[30] All non-hydrogen atoms were refined by using an anisotropic model. Hydrogen atoms were refined at calculated positions using a riding model. Powder diffraction data were collected in flat plate mode on a Bruker D8 Advance with monochromated Cu-Kα radiation (λ = 1.54056 Å) in reflection geometry at 298 K. Variable-temperature PXRD data were obtained using the SuperNova with Cu-Kα radiation set to powder mode. A sample composed of unground dried crystallites was mounted in a rotating capillary placed in the temperature-controlled nitrogen flow of the cryostream. Crystallographic data for compounds **1** and **2** are available

free of charge from the Cambridge Crystallographic Data Centre under the codes CCDC 1519562-1519563.

Quantum-chemical modelling. Molecular calculations were carried out on the pyrazine molecule and pyz-Ag adduct using Gaussian 09.[31] The calculations were performed with the PBE0 functional[32] and Pople split-valence sets[33] of 6-31g and 6-31g** quality for the H and C/N atoms, respectively, with the LANL2DZ effective-core pseudopotential[34] and corresponding double-zeta basis set being used for Ag. Structural optimisations were performed using the default convergence criteria, and successful optimisation confirmed by the absence of imaginary vibrational modes. Periodic calculations were performed on **1**, **2** and **3** using the plane-wave pseudopotential density-functional theory (DFT) formalism implemented in the Vienna *Ab initio* Simulation Package (VASP).[35] The X-ray structures of the three materials were fully relaxed (i.e. internal positions and cell shape/volume) until the magnitude of the forces on the ions fell below 10^{-2} eV $Å^{-1}$. The optimised lattice parameters are listed in the extended data. The PBEsol generalized-gradient approximation functional[35] with the DFT-D3 dispersion correction[36] was employed alongside projector augmented-wave (PAW) pseudopotentials[37] treating the C, N and O 2s and 2p and the Ag 5s, 4d and 4p electrons as valence. A plane-wave cutoff of 850 eV was used in conjunction with Γ-centered Monkhorst-Pack *k*-point meshes with 3×3×1, 3×3×3 and 3×3×3 subdivisions for **1**, **2** and **3**, respectively, to integrate the electronic Brillouin zones. These convergence criteria were sufficient to converge the absolute values of the total energy and external pressure to well within 1 meV $atom^{-1}$ and 1 kbar (0.1 GPa), respectively. A tolerance of 10^{-8} eV was applied during the minimisation of the electronic wavefunctions. The absorption spectra of the three models were calculated from the PBEsol-D3-optimised structures using the PBE0 hybrid exchange-correlation functional[32] and the linear-optics routines in VASP.[38] For these calculations, the Niggli-reduced cell of **3** was used with a 3×3×3 *k*-point mesh, and the number of electronic bands in the three models was increased to 360 (**1**) and 180 (**2**/**3**), which is roughly 2× the default in all three cases, to ensure convergence of the sum over empty states.

Acknowledgements

The authors gratefully acknowledge support from an EPSRC programme grant (grant no. EP/K004956/1). The computational modelling was carried out using the SiSu supercomputer at the IT Center for Science (CSC), Finland, via the Partnership for Advanced Computing in Europe (PRACE) project no. 13DECI0317/IsoSwitch. Some calculations were also performed on the Balena HPC facility at the University of Bath, which is maintained by the Bath University Computing Services. Data from the computational modelling, including the optimised structures of **1**, **2** and **3** and the simulated absorption spectra, are available free of charge from an online repository at [TODO: URL to be added on acceptance].

Keywords: anion···π interactions • metastability • coordination polymers • silver • single-crystal-to-single-crystal transformation

[1] D. Quiñonero, C. Garau, C. Rotger, A. Frontera, P. Ballester, A. Costa, P. M. Deyà, *Angew. Chem. Int. Ed.* **2002**, *41*, 3389-3392.

[2] R. E. Dawson, A. Hennig, D. P. Weimann, D. Emery, V. Ravikumar, J. Montenegro, T. Takeuchi, S. Gabutti, M. Mayor, J. Mareda, C. A. Schalley, S. Matile, *Nat. Chem.* **2010**, *2*, 533-538.

[3] D.-X. Wang, M.-X. Wang, *J. Am. Chem. Soc.* **2013**, *135*, 892-897.

[4] D. Quiñonero, A. Frontera, P. M. Deyà, *ChemPhysChem* **2008**, *9*, 397-399.

[5] S. Kozuch, *Phys. Chem. Chem. Phys.* **2016**, *18*, 30366-30369.

[6] X. Lucas, A. Bauzá, A. Frontera, D. Quiñonero, *Chem. Sci.* **2016**, *7*, 1038-1050.

[7] Y. Zhao, C. Beuchat, Y. Domoto, J. Gajewy, A. Wilson, J. Mareda, N. Sakai, S. Matile, *J. Am. Chem. Soc.* **2014**, *136*, 2101-2111.

[8] (a) J. T. Davis, *Nat. Chem.* **2010**, *2*, 516-517. (b) A. V. Jentzsch, D. Emery, J. Mareda, P. Metrangolo, G. Resnati, S. Matile, *Angew. Chem. Int. Ed.* **2011**, *50*, 11675-11678.

[9] (a) A. Frontera, P. Gamez, M. Mascal, T. J. Mooibroek, J. Reedijk, *Angew. Chem. Int. Ed.* **2011**, *50*, 9564-9583. (b) N. Hafezi, J. M. Holcroft, K. J. Hartleib, E. J. Dale, N. A. Vermeulen, C. L. Stern, A. A. Sarjeant, J. F. Stoddart, *Angew. Chem. Int. Ed.* **2015**, *127*, 466-471. (c) O. Perraud, V. Robert, H. Gornitzka, A. Martinez, P. Dutasta, *Angew. Chem. Int. Ed.* **2012**, *51*, 504-508.

[10] B. P. Hay, R. Custelcean, *Cryst. Growth & Des.* **2009**, *9*, 2539-2545.

[11] (a) L. Brammer, M. D. Burgard, C. S. Rodger, J. K. Swearingen, N. P. Path, *Chem. Commun.* **2001**, 2468-2469. (b) R. G. Vranka, E. L. Amma, *Inorg. Chem.* **1966**, *5*, 1020-1025. (c) F. F. Li, J.-F. Ma, S.-Y. Song, J. Yang, Y.-Y. Liu, Z.-M. Su, *Inorg. Chem.* **2005**, *44*, 9374-9383. (d) S. R. Batten, B. F. Hoskins, R. Robson, *New J. Chem.* **1998**, *22*, 173-175. (e) L. Carlucci, G. Ciani, D. M. Proserpio, A. Sironi, *Angew. Chem. Int. Ed.* **1995**, *34*, 1895-1898. (f) L. Carlucci, G. Ciani, D. M. Proserpio, A. Sironi, *J. Am. Chem. Soc.* **1995**, *117*, 4562-4569. (g) P. J. Steel, C. J. Sumby, *Dalton Trans.* **2003**, 4505-4515. (h) N. Schultheiss, D. R. Powell, E. Bosch, *Inorg. Chem.* **2003**, *42*, 8886-8890.

[12] G. Meyer, M. Sehabi, I. Pantenburg in *Coordinative Flexibility of Monovalent Silver in [Ag1←L1]L2 Complexes in Design and Construction of Coordination Polymers*, (Eds.: M.-C. Hong, L. Chen), John Wiley & Sons, Inc., New Jersey, **2009**.

[13] M. B. Duriska, S. R. Batten, D. J. Price, *Aus. J. Chem.* **2006**, *59*, 26-29.

[14] T. M. Garrett, U. Koert, J.-M. Lehn, A. Rigault, D. Meyer, J. Fischer, *J. Chem. Soc., Chem. Commun*. **1990**, 557-558.

[15] (a) A. J. Blake, N. R. Champness, A. N. Khlobystov, D. A. Lemenovskii, W.-S. Li, M. Schröder, *Chem. Commun.* **1997**, 1339-1340. (b) K. Chainok, S. M. Neville, C. M. Forsyth, W. J. Gee, K. S. Murray, S. R. Batten, *CrystEngComm* **2012**, *14*, 3717-3726. (c) A. J. Blake, N. R. Champness, M. Crew, S. Parsons, *New J. Chem.* **1999**, 13-15.

[16] J. V. Knichal, W. J. Gee, C. A. Cameron, J. M. Skelton, K. J. Gagnon, S. J. Teat, C. C. Wilson, P. R. Raithby, A. D. Burrows, *Eur. J. Inorg. Chem.* **2017**, *accepted*.

[17] (a) M. A. Kalinina, *Colloid Journal* **2015**, *77*, 537-555. (b) P. Gütlich, Y. Garcia, T. Woike, *Coord. Chem. Rev.* **2001**, *219*, 839-879. (c) J. Gopalakrishnan, *Chem. Mater.* **1995**, *7*, 1265-1275. (d) H. Jones, *Rep. Prog. Phys.* **1973**, *36*, 1425-1485.

[18] (a) J. Holaň, E. Skořepová, L. Heraud, D. Baltes, J. Rohlíček, O. Dammer, L. Ridvan, F. Stěpánek, *Org. Process Res. Dev.* **2016**, *20*, 33-43. (b) Y. Zhang, Y. B. Jiang, D. K. Zhang, Y. Qian, X. Z. Wang, *Chem. Eng. Res. Des.* **2015**, *95*, 187-194.

[19] (a) J. M. Cole, *Analyst* **2011**, *136*, 448-455. (b) L. E. Hatcher, P. R. Raithby, *Coord. Chem. Rev.* **2014**, *277-278*, 69-79.

[20] (a) M. A. Halcrow, *Chem. Soc. Rev.* **2011**, *40*, 4119-4142. (b) Y.-M. Song, F. Luo, M.-B. Luo, Z.-W. Liao, G.-M. Sun, X.-Z. Tian, Y. Zhu, Z.-J. Yuan, S.-J. Liu, W.-Y. Xu, X.-F. Feng, *Chem. Commun.* **2012**, *48*, 1006-1008.

[21] (a) J. V. Knichal, W. J. Gee, A. D. Burrows, P. R. Raithby, S. J. Teat, C. C. Wilson, *Chem. Commun.* **2014**, *50*, 14436-14439. (b) J. V. Knichal, W. J. Gee, A. D. Burrows, P. R. Raithby, C. C. Wilson, *Cryst. Growth Des.* **2015**, *15*, 465-474.

[22] (a) M. R. Warren, S. K. Brayshaw, A. L. Johnson, S. Schiffers, P. R. Raithby, T. L. Easun, M. W. George, J. E. Warren, S. J. Teat, *Angew. Chem. Int. Ed.* **2009**, *48*, 5711-5714. (b) J. M. Skelton, R. Crespo-Otero,

L. E. Hatcher, S. C. Parker, P. R. Raithby, A. Walsh, *CrystEngComm* **2015**, *17*, 383-394.
[23] I. Persson, K. B. Nilsson, *Inorg. Chem.* **2006**, *45*, 7428-7434.
[24] H. Ito, M. Muromoto, S. Kurenuma, S. Ishizaka, N. Kitamura, H. Sato, T. Seki, *Nat. Commun.* **2013**, *4*, 1-5.
[25] R. Díaz-Torres, S. Alvarez, *Dalton Trans.* **2011**, *40*, 10742-10750.
[26] (a) M.-C. Hong, L. Chen in *Design and Construction of Coordination Polymers*, John Wiley & Sons, Inc., New Jersey, **2009**. (b) S. L. Price, *Chem. Soc. Rev.* **2014**, *43*, 2098-2111.
[27] T. Threlfall, *Org. Proc. Res. Dev.*, **2003**, 7, 1017-1027.
[28] L. J. Barbour, *J. Supramol. Chem.* **2001**, *1*, 189-191.
[29] G. M. Sheldrick, *Sect. A: Found. Crystallogr.* **2008**, *a64*, 112-122.
[30] G. M. Sheldrick, *Acta Cryst.* **2015**, *C. 71*, 3-8.
[31] *Gaussian 09*, Revision E.01, M. J. Frisch, G. W. Trucks, H. B. Schlegel, G. E. Scuseria, M. A. Robb, J. R. Cheeseman, G. Scalmani, V. Barone, B. Mennucci, G. A. Petersson, H. Nakatsuji, M. Caricato, X. Li, H. P. Hratchian, A. F. Izmaylov, J. Bloino, G. Zheng, J. L. Sonnenberg, M. Hada, M. Ehara, K. Toyota, R. Fukuda, J. Hasegawa, M. Ishida, T. Nakajima, Y. Honda, O. Kitao, H. Nakai, T. Vreven, J. A. Jr. Montgomery, J. E. Peralta, F. Ogliaro, M. Bearpark, J. J. Heyd, E. Brothers, K. N. Kudin, V. N. Staroverov, R. Kobayashi, J. Normand, K. Raghavachari, A. Rendell, J. C. Burant, S. S. Iyengar, J. Tomasi, M. Cossi, N. Rega, J. M. Millam, M. Klene, J. E. Knox, J. B. Cross, V. Bakken, C. Adamo, J. Jaramillo, R. Gomperts, R. E. Stratmann, O. Yazyev, A. J. Austin, R. Cammi, C. Pomelli, J. W. Ochterski, R. L. Martin, K. Morokuma, V. G. Zakrzewski, G. A. Voth, P. Salvador, J. J. Dannenberg, S. Dapprich, A. Daniels, Ö. Farkas, J. B. Foresman, J. V. Ortiz, J. Cioslowski, D. J. Fox, Gaussian, Inc., Wallingford CT, **2009**.
[32] C. Adamo, V. Barone, *J. Chem. Phys*. **1999**, *110*, 6158-6170.
[33] R. Ditchfield, W. J. Hehre, J. A. Pople, *J. Chem. Phys.* **1971**, *54*, 724-728.
[34] P. J. Hay, W. R. Wadt, *J. Chem. Phys.* **1985**, *82*, 270-283.
[35] G. Kresse, J. Hafner, *Phys. Rev. B* **1993**, *47*, 558-561.
[36] S. Grimme, J. Antony, S. Ehrlich, H. Krieg, *J. Chem. Phys.* **2010**, *132*, 154104.
[37] (a) P. E. Blöchl, *Phys. Rev. B* **1994**, *50*, 17953-17979; (b) G. Kresse, D. Joubert, *Phys. Rev. B* **1999**, *59*, 1758-1775.
[38] M. Gajdoš, K. Hummer, G. Kresse, J. Furthmüller, F. Bechstedt, *Phys. Rev. B* **2006**, *73*, 045112.

Entry for the Table of Contents (Please choose one layout)

Layout 2:

FULL PAPER

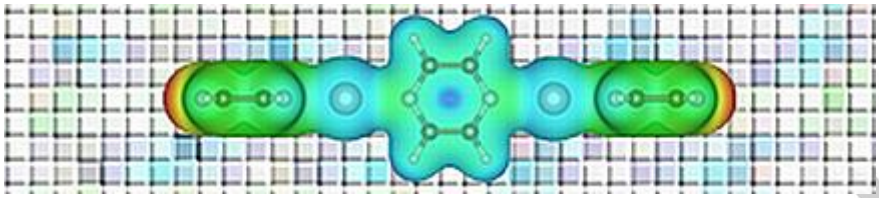

Humble pie: Anion···π interactions are shown here to play a key role in facilitating a cascade of single-crystal-to-single-crystal transformations. These new silver-pyrazine metastable materials exhibit responsiveness towards temperature and specific solvent vapours, and detailed X-ray diffraction and computational investigations provide insights into a plausible solid-state conversion mechanism.

William J. Gee, Karen Robertson and Jonathan M. Skelton*

Page No. – Page No.

Anion···π interactions and metastability: structural transformations in a silver-pyrazine network